Divalent Cation-Dependent Formation of Electrostatic PIP_2 Clusters in Lipid Monolayers

Wouter G. Ellenbroek,[†‡△*] Yu-Hsiu Wang,[§△] David A. Christian,[¶] Dennis E. Discher,[¶] Paul A. Janmey,[†‖***] and Andrea J. Liu[†§*]

[†]Department of Physics and Astronomy, University of Pennsylvania, Philadelphia, Pennsylvania; [‡]Department of Applied Physics and Institute for Complex Molecular Systems, Eindhoven University of Technology, Eindhoven, The Netherlands; [§]Department of Chemistry, [¶]Department of Chemical and Biomolecular Engineering, [‖]Institute for Medicine and Engineering, and **Departments of Physiology and Bioengineering, University of Pennsylvania, Philadelphia, Pennsylvania

ABSTRACT Polyphosphoinositides are among the most highly charged molecules in the cell membrane, and the most common polyphosphoinositide, phosphatidylinositol-4,5-bisphosphate (PIP_2), is involved in many mechanical and biochemical processes in the cell membrane. Divalent cations such as calcium can cause clustering of the polyanionic PIP_2, but the origin and strength of the effective attractions leading to clustering has been unclear. In addition, the question of whether the ion-mediated attractions could be strong enough to alter the mechanical properties of the membrane, to our knowledge, has not been addressed. We study phase separation in mixed monolayers of neutral and highly negatively charged lipids, induced by the addition of divalent positively charged counterions, both experimentally and numerically. We find good agreement between experiments on mixtures of PIP_2 and 1-stearoyl-2-oleoyl phosphatidylcholine and simulations of a simplified model in which only the essential electrostatic interactions are retained. In addition, we find numerically that under certain conditions the effective attractions can rigidify the resulting clusters. Our results support an interpretation of PIP_2 clustering as governed primarily by electrostatic interactions. At physiological pH, the simulations suggest that the effective attractions are strong enough to give nearly pure clusters of PIP_2 even at small overall concentrations of PIP_2.

INTRODUCTION

The concentration of the lipid phosphatidylinositol-4,5-bisphosphate (PIP_2) in the cell membrane is only of ~1%, yet it plays an outsized role in many critical processes, including cell division (1), endocytosis and exocytosis (2), and cell motility (3). Evidence exists that PIP_2 forms clusters (4) at the submicron scale in vitro, and it has been speculated that similar domains might form under roughly physiological conditions. It has been conjectured that this clustering is crucial to its function at such low concentration (5,6).

Various mechanisms for the clustering have been proposed, including PIP_2-protein interactions (7,8), exclusion from cholesterol-enriched ordered domains (4,9), and hydrogen bonds (10,11). However, recent experiments showed that PIP_2 clusters can also be induced simply by adding calcium or other divalent ions (4,12). This raises the question of whether a purely electrostatic, ion-mediated mechanism could cause PIP_2 clustering.

A counterion-mediated mechanism would seem unlikely because such attractions are typically quite weak. Biomolecules such as DNA (13) and actin (14) aggregate into large bundles in the presence of multivalent ions, but they each carry a net charge of ($\sim -10^2$–$10^3 e$) while PIP_2 lipids carry a much smaller net charge ($\sim 3e$). Moreover, divalent cations are not sufficient to induce aggregation in bulk aqueous DNA or actin solutions, and the estimated attraction mediated by trivalent or tetravalent species is at most of ~0.1 k_BT per basepair (15). This small magnitude is not surprising because counterion-mediated attractions vanish in the mean-field approximation (16) and are the collective result of a near-cancellation of repulsive and attractive interactions between like and unlike charges, respectively. We note that the near-cancellation implies that the geometry of the charge configuration is likely to be important so that attractions mediated by small ions such as calcium can behave very differently from those mediated by extended cationic molecules such as spermidine (17).

In this article, we show that ion-mediated attractions in low-charged objects such as lipids are surprisingly strong, so that phase separation not only occurs but can be nearly complete at physiological values of the PIP_2 charge. We conduct simulations on a model designed to retain only the most critical features of the electrostatics and compare the results to experiments on Langmuir monolayers of a mixture of PIP_2 with neutral lipids with added divalent salts. We find semiquantitative agreement between simulations and experiments, suggesting that divalent-ion-mediated attractions are responsible for the observed clustering. The strength of these interactions depends strongly on the net charge of the lipid, which in turn has

Submitted June 22, 2011, and accepted for publication September 19, 2011.

△Wouter G. Ellenbroek and Yu-Hsiu Wang contributed equally to this work.

*Correspondence: w.g.ellenbroek@tue.nl or ajliu@physics.upenn.edu or janmey@mail.med.upenn.edu

Editor: Reinhard Lipowsky.

0006-3495/11/11/2178/7 $2.00

doi: 10.1016/j.bpj.2011.09.039

been shown to depend sensitively on ionic strength and on pH within a physiological range (18).

In addition, the simulations provide, to our knowledge, new insight into the mechanical properties of ion-mediated clusters: at moderate PIP_2 charge, they are like two-dimensional liquids in which lipids can diffuse around as usual, but at sufficiently high PIP_2 charge they form rigid, gel-like clusters upon exposure to divalent ions.

MATERIALS AND METHODS

Experiments

We look for phase separation using visual analysis of both epifluorescence micrographs and atomic force micrographs of mixed lipid monolayers prepared in a Langmuir trough (Kibron, Helsinki, Finland). L-α-phosphatidylinositol-4,5-bisphosphate (PIP_2) and 1-stearoyl-2-oleoyl phosphatidylcholine (SOPC) were purchased from Avanti Polar Lipids (Alabaster, AL). In the epifluorescence studies, part of the PIP_2 (equal to 0.5 mol % of the total lipid content) is replaced by a fluorescently labeled analog (BODIPY FL-PIP_2), purchased from Echelon (Salt Lake City, UT).

The lipid mixture, consisting of SOPC with a total molar PIP_2 fraction of ϕ_{PIP} is dissolved in a 2:1 chloroform/methanol mixture. A lipid monolayer is formed on a buffered subphase (10 mM HEPES, 100 μM EDTA, 5 mM DTT) by addition of the lipid solution to the air-water interface. The surface pressure is kept at 20 mN/m, corresponding to an initial area per lipid of ~90 $Å^2$.

In the fluorescence studies the monolayer is imaged on an inverted epifluorescence microscope, using the 10× objective. We verify that there are at most two bright spots, likely due to nonspecific insoluble aggregates or contaminants, in a field of view at this stage. The divalent salts $CaCl_2$ or $MgCl_2$ are then added at 1 mM to the subphase, followed by gentle mixing to avoid disrupting the monolayer. We allow up to 2 h for domains to coarsen before imaging again.

For the AFM studies, sample preparation is identical with the exception that the buffer in this case contains only 1 μM EDTA. Monolayer samples are transferred from the trough onto a glass coverslip, both before and after addition of divalent salt. These films are imaged on a NanoScope III atomic force microscope (Digital Instruments, Tonawanda, NY) in tapping mode.

We perform these procedures for a range of ϕ_{PIP}-values and several pH values: 3, 4.5, 6, 7.4, and 9. At these values of the pH, q_{PIP} is roughly −1.5, −2.7, −3.2, −4.2, and −5.0, respectively, based on acid dissociation constants from Levental et al. (18). However, the ionization state of PIP_2 may be influenced by various geometric and chemical factors (18,19), so we do not assume that these q_{PIP} values are exact. We collect the results in a phase diagram for each experiment: The fluorescence measurements are the most direct visualization of domains, but might miss the smallest domains because of limited resolution, while the AFM images provide a more detailed picture at smaller length scales.

Simulations

We retain only the competition between electrostatic interactions and excluded volume repulsions by adopting a model in which both lipids and small ions are represented as charged spheres (radius R_i) with an excluded volume interaction given by the purely repulsive (truncated at its minimum and shifted) Lennard-Jones potential (the WCA potential (20)). Parameterized by an energy scale $\varepsilon = k_BT \equiv 1$ (our unit of energy) and length scale $\sigma_{ij} = R_i + R_j$, this potential is given by

$$V_{WCA,ij}(r_{ij}) = 4\epsilon\left[\left(\frac{\sigma_{ij}}{r_{ij}}\right)^{12} - \left(\frac{\sigma_{ij}}{r_{ij}}\right)^{6} + \frac{1}{4}\right],$$

for $r_{ij} < 2^{1/6}\,\sigma_{ij}$, and $V(r_{ij}) = 0$ otherwise, where r_{ij} is the center-to-center distance. Note that σ_{ij} is the distance at which the potential equals k_BT. $N = 1600$ lipid particles are confined to the $z = 0$ plane, to mimic the effect of the hydrophobic interaction that keeps them at the air-water interface. We use $R_i = R_L = 3$ Å for the lipids and $R_i = R_{CI} = 2$ Å for the small cations that can explore the entire simulation box. In a study of the dependence of the clustering on cation size, we vary it between $0.5\ Å \le R_{CI} \le 2.5\ Å$. The box is periodic in x- and y-directions (size $L_x = 320\ Å \times L_y = 320\ Å$ and has hard walls at $z = 0$ and $z = L_z = 200$ Å. The typical distance between lipids in the monolayer at $z = 0$ is therefore 8 Å.

In addition, the charged spheres interact via the Coulomb interaction, $V_{C,ij} = q_iq_jl_B/r_{ij}$, where we measure charges q in units of the proton charge. In room temperature water the Bjerrum length $l_B \approx 7$ Å.

We run molecular-dynamics simulations using LAMMPS (21), with a Nosé-Hoover thermostat (22) and PPPM for the long-range Coulomb interactions (23).

The strong Coulomb attraction between the anionic lipids and the small cations allows them to bind at a distance of roughly σ_{ij}. The essence of ion-mediated attractions is that these bonds are strong and long-lived enough so that one or two counterions can draw together two lipids and be bound to both simultaneously (24,25). Due to its coarse-grained nature, our model underestimates the binding energy of such bonds. The main source of this effect is that the distance between the lipid particle and the Ca^{2+} in our model is much larger than the distance between a real phosphate group and a Ca^{2+} ion in real PIP_2. This common side-effect of coarse-graining is typically compensated by adjusting the dielectric constant (see, e.g., Marrink et al. (26)). To find the required correction, we compare the PIP_2 charge required for clustering as calculated from the numerical model and as measured in our experiments, at PIP_2 fraction $\phi_{PIP} = 0.25$. Experimentally we find the threshold pH at this PIP_2 fraction to be between 3 and 4.5, which corresponds to a charge of roughly $q_{PIP} \approx -2$ (18). The dielectric constant required in our model to match this threshold is ~27 (a factor-three lower than that of water). We then use this value of the dielectric constant to obtain the rest of the phase diagram.

Thus, we have a coarse-grained model in which lipids are replaced by spheres of the appropriate charge and simulated with explicit counterions using an adjusted dielectric constant. This simplification enables us to explore a large parameter space with modest computations. Of course, this coarse-graining approach is not quantitatively precise, but neither are calculations using typical approximations such as a uniform dielectric constant of 80 for water surrounding highly charged objects. We note that despite the simplicity of our model, it gives surface pressures of ~20–50 mN/m, which is of the same order as in the experiments. Both in the experiments and in the simulations, the surface pressure drops by a few percent at low ϕ_{PIP}, and between 10% and 30% at $\phi_{PIP} = 0.25$, upon addition of Ca^{2+}.

These simulations were performed for a range of PIP_2 charges q_{PIP} and PIP_2 fractions ϕ_{PIP}. To study the mobility of lipids within clusters and the cluster rigidity, we performed additional simulations at $\phi_{PIP} = 1$.

RESULTS

Phase behavior: experiments and simulation

Fig. 1 shows our experimental results: phase diagrams and snapshots of AFM (Fig. 1 *a*) and fluorescence (Fig. 1 *b*) studies of calcium-induced domain formation. At high PIP_2 charge, cluster formation is readily observed, for example at pH 7.4 in either experiment, where $q_{PIP} \approx -4.2$ (Fig. 1, *a 2*, *a 3*, and *b*). Fig. 1 *b* shows epifluorescence micrographs, taken both before (*left*) and after (*right*) transferring the sample to a glass coverslip, at 25% PIP_2 and pH 7.4. In these images, bright spots mark regions where PIP_2 is concentrated. In the phase diagram, conditions for which

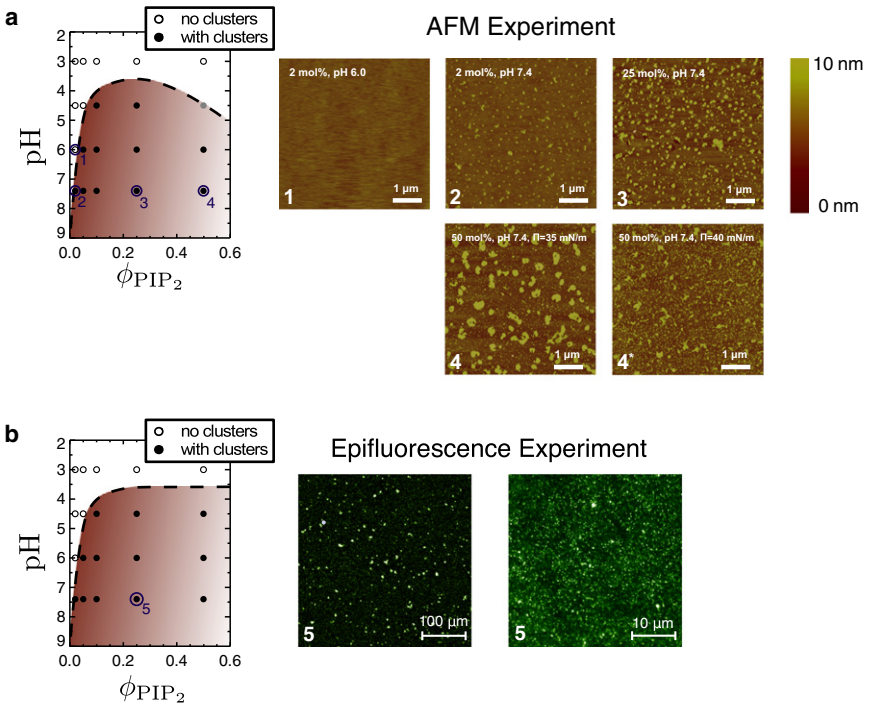

FIGURE 1 Phase diagrams (pH versus PIP_2 fraction) and snapshots of experiments on mixed lipid monolayers (containing SOPC and PIP_2) exposed to divalent salt. (*a*) Phase diagram. (*Shaded coexistence region*) Where clustering was observed, obtained from AFM studies. (*Open disks*) Parameter values where no clustering was observed. (*Shaded disks* are too close to the boundary to determine their behavior with certainty.) The AFM snapshots *1*, *2*, and *3* represent the conditions indicated by the corresponding points in the diagram: At $\phi_{PIP} = 0.02$, there is no cluster formation at pH 6 but clusters are clearly present at pH 7.4. Larger domains are obtained for $\phi_{PIP} = 0.25$. Domains persist when the surface pressure Π is increased to 35 or 40 mN/m (panels *4* and *4**). (*b*) A very similar cluster formation phase diagram is obtained using epifluorescence with labeled PIP_2. Snapshots are shown for $\phi_{PIP} = 0.25$. (*Left snapshot*) Taken directly in the Langmuir trough. (*Right snapshot*) Taken after transferring the sample to a glass coverslip. We note that the apparent area fraction in the image is <0.25 because many of the PIP_2 domains are too small to detect optically.

these bright spots are seen are marked with solid disks. Cases that did not show signs of clustering are marked with open circles.

We note that domains usually appear within minutes, but we allow coarsening for up to 2 h before concluding there is no clustering. Thus we obtain the boundaries of the parameter region that lead to domain formation (*shaded* in the *phase diagram*). Fig. 1 *a* shows AFM images of the transferred samples. These images show a clear distinction between conditions that lead to domain formation (panels *a 2* and *a 3*) and conditions in which the AFM image is flat (panel *a 1*). Control AFM images of samples without divalent salt did not show any sign of domain formation either. Domains persist when the surface pressure is increased to 35 or 40 mN/m (panels *a 4* and *a 4**, respectively).

Although the two experimental approaches probe the system on different length scales, both of them give the same phase diagram. The exception is one data point, at pH 4.5 and $q_{PIP} = 0.5$, which showed clustering in the fluorescence experiments, but which were not as clearly clustered as the other data points in the AFM experiments (marked with a *shaded dot* in the phase diagram). We note that, in general, the AFM images are less noisy and therefore lead to a more clear-cut distinction between clustering and nonclustering conditions.

The simulation snapshot in Fig. 2 *c*, obtained after simulating for 3.5 ns using 25% PIP_2 with charge $q_{PIP} = -4$, shows still-growing clusters at a scale of ~10 nm. As expected, the positions of the condensed calcium ions (*red disks* in Fig. 2 *c*) clearly indicate their role in binding the charged lipids (*green disks*) together. To map out the phase diagram in the simulations, we follow the coarsening dynamics by keeping track of the static structure factor of the charged lipids,

$$S(\mathbf{k}) = \frac{1}{N}\sum_{i,j}^{N} \exp\left[i\mathbf{k}\cdot\left(\mathbf{r}_i - \mathbf{r}_j\right)\right],$$

where N is the number of PIP_2 particles. As a function of $k \equiv |\mathbf{k}|$, a maximum in this function at $k = k_{peak}$ indicates that the PIP_2 positions are developing structure at a length scale $2\pi/k_{peak}$. For the more pronounced cases of cluster formation (deep in the phase-separated regime), we followed this peak as a function of time and verified that it scales with time as $k_{peak} \sim t^{-1/3}$, consistent with the general theory of coarsening of a binary fluid mixture (27). Thus, even though the counterion-mediated origin of phase separation yields irregularly shaped clusters instead of circular ones, this does not seem to affect the kinetics of coarsening. In the phase diagram in Fig. 2 *a*, all parameter values (ϕ_{PIP}, q_{PIP}) for which an appreciable peak appears that approaches $k_{peak} = 0$ in $S(k)$ for long times were marked as cluster-forming (within the coexistence region). Both in the experiment and simulation, we found that divalent cations cause phase separation when the lipid charge is high enough (pH 4.5 or higher in experiment, $q_{PIP} \leq -2$ in simulation). Monovalent cations were never seen to induce clusters.

Larger divalent ions than Ca^{2+} should mediate weaker attractions, because larger binding distances imply lower

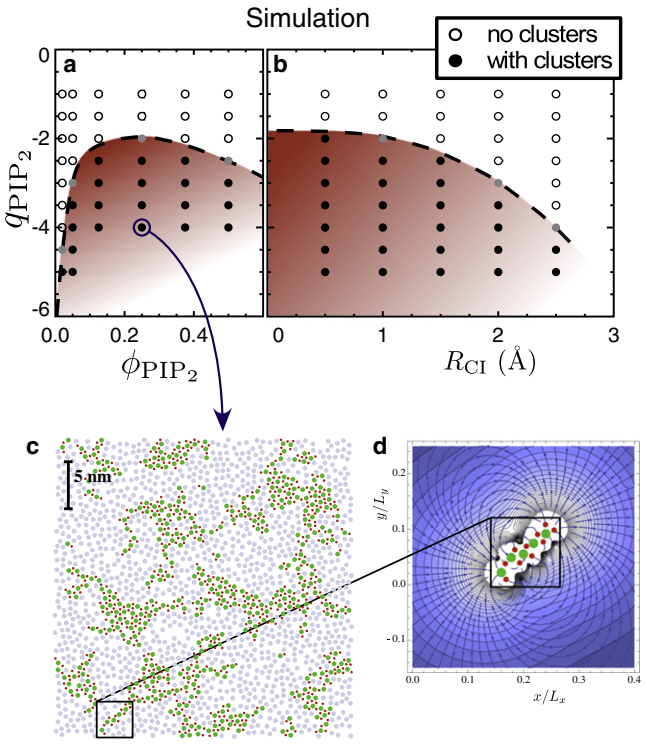

FIGURE 2 Phase diagram (charge versus PIP_2-fraction) and snapshots from simulation of charged-neutral mixed lipid monolayers exposed to divalent salt. (*a*) Phase diagram obtained using a divalent ion radius $R_{CI} = 2$ Å. (*Solid disks* in the *shaded coexistence region*) Where clustering was observed. (*Open circles*) Mixed samples. (*Gray disks* are too close to the boundary to determine their behavior with certainty.) (*b*) Larger divalent ions require a higher lipid charge to induce clustering (shown for $\phi_{PIP} = 0.05$). (*c*) The simulation (PIP_2 charge $q_{PIP} = -4$, PIP_2 fraction $\phi_{PIP} = 0.25$, and divalent ion radius $R_{CI} = 2$ Å) after 3.5 ns of coarsening. Charged and neutral lipids are dark green and light gray discs, respectively, and divalent ions that are close to the lipid monolayer are indicated with smaller dark red dots. (*d*) Strength (*shaded contours*) and direction (*streamlines*) of the electric field around a stringlike domain taken from the simulation, illustrating that further growth of the domain is likely to occur at the end.

Coulomb energies. This effect should manifest itself in a higher charge on the PIP_2 needed to obtain cluster formation with larger ions. We verified this in experiments at $q_{PIP} = 0.25$ using Mg^{2+}, which has a larger hydrated radius than Ca^{2+}, although the precise values are uncertain (note that the reported hydrated radii vary, mainly due to different methods to determine them, but Mg^{2+} is consistently larger (3–7 Å) than Ca^{2+} (2.6–6.3 Å) (28–30)). We find that Mg^{2+} only induces clusters if pH $\geq$ 6 while Ca^{2+} already does it at pH 4.5. In agreement with this observation, the ability of divalent cations to drive cluster formation in our simulations also decreases with increasing ion size (Fig. 2 *b*).

Cluster morphology

The morphology observed in the early stages of coarsening in the simulations illustrates some particular features of ion-mediated attractions. The PIP_2-rich clusters (see Fig. 2 *c*) are often irregularly shaped, and even stringlike. This occurs because the attraction, of the order of a few k_BT, is the net result of strong attractions (PIP_2-Ca^{2+}) and strong repulsions (PIP_2-PIP_2 and Ca^{2+}-Ca^{2+}) that can each be several tens of k_BT.

In the earliest stages of coarsening, most domains are stringlike, because for very small clusters such linear arrangements have the lowest Coulomb energy. As the domains grow, compact shapes become energetically favorable but are difficult to reach for two kinetic reasons: First, once there is a stringlike cluster, the electric field in its neighborhood is focused toward the end of the string (see Fig. 2 *d*), making it more likely for the next lipid to bind at the end, thus extending the string. Second, any rearrangement of the lipids requires the nearby counterions to move aside, which involves energy barriers of the order of the bare (tens of k_BT) interactions. As a result, the evolution toward more compact shapes is severely hindered kinetically, and irregularly shaped domains, which have also been seen experimentally (4,7), can persist even in the later stages of coarsening (Fig. 2 *c*). This observation also strongly suggests that irregularly shaped clusters are gel-like because diffusion of lipids within the cluster should be hindered by the same energy barriers.

Cluster rigidity

For those PIP_2 charges at which cluster formation was observed, additional simulations at $q_{PIP} = 1$ provide information on cluster rigidity or gelation. As shown in Fig. 3 *a*, we find from the mean-square displacement that at $q_{PIP} \leq -3.5$, the PIP_2 do not diffuse over the course of the simulation (corresponding to 3.5 ns), indicating that clusters are mechanically rigid on that timescale. At $q_{PIP} \geq -2.5$, on the other hand, the lipids diffuse around freely, indicating that the clusters are fluid. These curves are averaged over five runs with identical parameters but different initial random conditions. At $q_{PIP} = 3$, the system appears to be marginally rigid on the timescale of our runs; the lipids diffuse in some runs but not in others.

Within a rigid cluster, each lipid has a well-defined average position about which it fluctuates thermally. What keeps them in place can be described as an effective interaction between nearby PIP_2 molecules, mediated by the divalent counterions. The strength of this effective interaction is obtained from the matrix of displacement correlations U, defined via

$$U_{ij} = \langle u_i(t) u_j(t) \rangle_t, \quad (1)$$

where $u_i(t)$ is the deviation of coordinate i from its average value at time t. Hence, U is $2N \times 2N$ for our two-dimensional system. When these deviations are small they explore the effective potential energy V_{eff} around its minimum, so we can describe it by a second-order Taylor expansion.

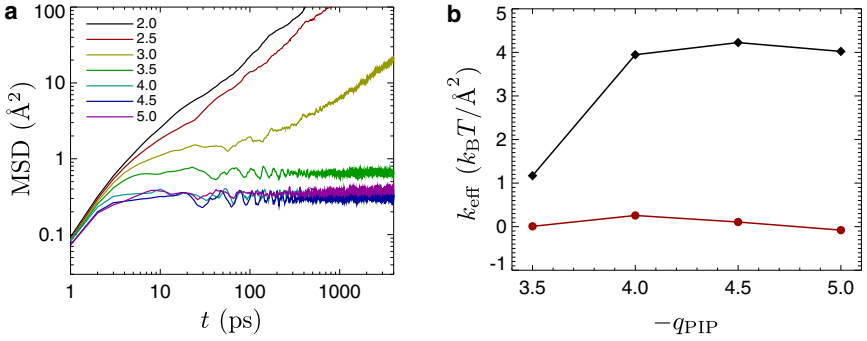

FIGURE 3 Diffusion and rigidity of lipids within PIP_2 domains at $\phi_{PIP} = 1$ and $R_{CI} = 1$ Å. (*a*) Mean-square displacement for lipids in a PIP_2-domain as a function of time, for various PIP_2 charges, as shown in the legend. For sufficiently negative PIP_2 charge, the domains are solid. (*b*) The stiffness of the effective harmonic interaction between neighboring PIP_2 molecules in the PIP_2 domain, obtained by displacement correlation analysis. (*Black diamonds*) Stiffness corresponding to normal (central) effective interactions. (*Red disks*) The (negligibly small) effective tangential stiffness.

This allows extraction of the dynamical matrix K of the system as the inverse of the correlation matrix,

$$\frac{\partial^2 V_{eff}}{\partial u_i \partial u_j} \equiv K_{ij} = k_{\rm B}T\left(U^{-1}\right)_{ij}, \qquad (2)$$

which can be obtained directly from the partition function (31). The elements of the dynamical matrix then provide the stiffness of the effective spring that acts between two neighboring PIP_2. The result is shown in Fig. 3 *b*: The tangential stiffness of the effective interaction between neighboring PIP_2 is negligible, indicating that the effective interaction does not prevent particles from sliding past each other, while the normal effective stiffness is ~4 $k_{\rm B}T$/Å^2 when $q_{\rm PIP} \leq -4$.

DISCUSSION

The two experiments yield nearly identical phase diagrams, showing clustering of PIP_2 for pH $\geq$ 4.5 at PIP_2 fractions at ~25%, a threshold which approaches pH 7.4 at PIP_2 fractions as low as 2%.

The phase diagram of our numerical model compares surprisingly well with the experiments. The only parameter we introduce is the dielectric correction factor, a usual necessity in coarse-grained simulations. It is fixed by comparing clustering at one packing fraction ($\phi_{PIP} = 0.25$), after which the rest of the phase diagram is reproduced without any free parameters.

It should be noted that, although hydrogen bonds between the PIP_2 molecules exist and may play a role when the charges are small (10), our work strongly suggests that they do not play a dominant role in multivalent ion-induced clustering—if they did, having a higher PIP_2 charge would make it harder to form clusters, rather than easier, as we report in Figs. 1 *a* and 2 *a*.

One might ask how relevant our results are to biological membranes. Most of our measurements are taken at a relatively low surface pressure of 20 mN/m to prevent barrier leakage of the lipids. However, the formation of domains persists when surface pressure is increased up to 35 or 40 mN/m (see Fig. 1 *a* 4), and between 20 and 35 mN/m the typical domain size even grows with surface pressure. This is a characteristic signature of domain formation driven by electrostatic correlations, because a denser aggregate containing charged lipids will attract more divalent ions. We also observed domains by AFM in monolayers containing 1% PIP_2 at 35 mN/m over subphases containing 150 mM KCl, pH 7.4, suggesting that even at roughly physiological conditions, Ca^{2+}-induced clustering can be relevant (Y.-H. Wang and P. A. Janmey, unpublished).

As for the use of monolayers instead of real membranes, we first note that PIP_2 in the cell membrane only resides on the inner leaflet. In addition, the use of monolayers will not significantly affect the electrostatics because distances between opposite charges are much smaller than the thickness of the low-dielectric layer of a membrane. However, an important limitation of monolayers in both experiment and simulation is that membrane curvature is not allowed. There might be changes in the exact concentrations or charges at which domains first form when membrane curvature is allowed, and indeed the cation-driven changes in surface pressure we measure on the PIP_2-containing leaflet might be enough to trigger local curvature in a bilayer.

Because the interactions in our model have been stripped down to the bare minimum of electrostatics and steric repulsion, the only attractive interaction in the simulations is the Coulomb attraction between PIP_2 and Ca^{2+}. Therefore, the observed phase separation must be due to counterion-mediated attractions. In both DNA solutions and in PIP_2, the negative charges come from phosphate groups and are typically several Å apart. For PIP_2, however, the net binding energy per lipid in 30-lipid clusters with Ca^{2+} is 6 $k_{\rm B}T$ for $q_{\rm PIP} \approx -3$, which is much stronger than in DNA (15). (This binding energy is calculated with respect to a reference state of 15 lipid dimers, neutralized with Ca^{2+}, so that the cluster is charge-neutral and monopole terms do not dominate the result.) This large difference must originate from rather subtle differences in the packing geometry of charges in the two cases. Chain connectivity of DNA prevents the charges from organizing in the low-energy

configurations that our lipids take (see Fig. 2 *c*), but instead forces both negative and positive charges into roughly linear arrangements (33), increasing repulsive contributions to the electrostatic energy and thereby weakening the effective attraction.

Although the binding energy between lipids in a cluster is a collective effect and can only be estimated with respect to a chosen reference state, the linearized effective interaction between neighboring PIP_2 is always well defined. One can think of this as the potential of mean force between PIP_2 that is left after integrating out the positions of the calcium ions, expanded around the average distance between the PIP_2 molecules involved. We determined the stiffness of the effective calcium-mediated bond between PIP_2 molecules to be ~4 $k_BT/Å^2$ for the case of gel-like clusters of highly charged PIP_2 ($q_{PIP} \leq -4$). This is approximately an order-of-magnitude lower than the stiffness with which a single Ca^{2+} is bound to a PIP_2 in our simulations, consistent with the notion that ion-mediated attractions are the result of near-cancellation of much stronger attractive and repulsive interactions. Yet at $q_{PIP} \leq -4$ the ion-mediated attractions are still strong enough to lead not only to phase separation, but also to mechanical rigidity in PIP_2-rich domains.

Whether or not this rigidifying effect could be noticeable in living cells is questionable. First, we note that the timescale of our simulations is of the order of nanoseconds; more highly negative values of q_{PIP} would be needed to achieve rigidity at longer timescales relevant to experiments and to biological processes. Second, other effects that were not included in our simulations—such as active processes (e.g., from molecular motors) and increased disorder (because real lipids are not spheres in a plane)—also act to drive the threshold value of q_{PIP} for rigidity beyond the physiological value of $q_{PIP} \approx -4$. We note that a similar calcium-induced gelation effect has been observed experimentally in polymer amphiphile systems (34). In that context, gelation is less surprising because the total charge per molecule is much higher for the polymer amphiphiles than for PIP_2.

In summary, we have presented experiments and coarse-grained simulations on lipid monolayers that demonstrate the clustering of PIP_2 in mixed monolayers via calcium-mediated electrostatic attractions. Furthermore, we detected a transition from fluid to gel domains as the charge on the PIP_2 increased, and obtained the conditions for cluster rigidity from the simulations. Between PIP_2 charges of -2 and -4, the strength of ion-mediated attractions is highly sensitive to the PIP_2 charge; they become strong enough to make long-lived cross-links between lipids when $q_{PIP} \approx -4$, as illustrated by the interaction stiffnesses in Fig. 3.

In all, our results suggest that at physiological pH the effective calcium-mediated attraction can drive the formation of fluid clusters of PIP_2 even at PIP_2 mole fractions of 2% or lower. In the cell, other factors such as the presence of other polycationic ligands, i.e., polyamines and protein domains, can also affect PIP_2 distribution; however, the clustering effect of Ca^{2+} is likely to remain a significant influence on PIP_2 distribution.

We thank I. Levental and A. Travesset for discussions.

This work was supported by the National Science Foundation through the UPenn Materials Research and Engineering Center under grant No. DMR-0520021, and grant No. DMR-0605044 to A.J.L.; by National Institutes of Health grant No. HL067286 to P.A.J.; and by the Netherlands Organisation for Scientific Research (NWO) through a Veni grant to W.G.E.

REFERENCES

1. Saul, D., L. Fabian, …, J. A. Brill. 2004. Continuous phosphatidylinositol metabolism is required for cleavage of crane fly spermatocytes. *J. Cell Sci.* 117:3887–3896.
2. Martin, T. F. J. 2001. PI(4,5)P(2) regulation of surface membrane traffic. *Curr. Opin. Cell Biol.* 13:493–499.
3. Janmey, P. A. 1994. Phosphoinositides and calcium as regulators of cellular actin assembly and disassembly. *Annu. Rev. Physiol.* 56:169–191.
4. Levental, I., D. A. Christian, …, P. A. Janmey. 2009. Calcium-dependent lateral organization in phosphatidylinositol 4,5-bisphosphate (PIP_2)- and cholesterol-containing monolayers. *Biochemistry.* 48:8241–8248.
5. Martin-Belmonte, F., A. Gassama, …, K. Mostov. 2007. PTEN-mediated apical segregation of phosphoinositides controls epithelial morphogenesis through Cdc42. *Cell.* 128:383–397.
6. Richer, S. M., N. K. Stewart, …, M. G. Oakley. 2009. High affinity binding to profilin by a covalently constrained, soluble mimic of phosphatidylinositol-4,5-bisphosphate micelles. *ACS Chem. Biol.* 4:733–739.
7. McLaughlin, S., and D. Murray. 2005. Plasma membrane phosphoinositide organization by protein electrostatics. *Nature.* 438:605–611.
8. Laux, T., K. Fukami, …, P. Caroni. 2000. GAP43, MARCKS, and CAP23 modulate PI(4,5)P(2) at plasmalemmal rafts, and regulate cell cortex actin dynamics through a common mechanism. *J. Cell Biol.* 149:1455–1472.
9. Levental, I., F. J. Byfield, …, P. A. Janmey. 2009. Cholesterol-dependent phase separation in cell-derived giant plasma-membrane vesicles. *Biochem. J.* 424:163–167.
10. Levental, I., A. Cebers, and P. A. Janmey. 2008. Combined electrostatics and hydrogen bonding determine intermolecular interactions between polyphosphoinositides. *J. Am. Chem. Soc.* 130:9025–9030.
11. Redfern, D. A., and A. Gericke. 2005. pH-dependent domain formation in phosphatidylinositol polyphosphate/phosphatidylcholine mixed vesicles. *J. Lipid Res.* 46:504–515.
12. Carvalho, K., L. Ramos, …, C. Picart. 2008. Giant unilamellar vesicles containing phosphatidylinositol(4,5)bisphosphate: characterization and functionality. *Biophys. J.* 95:4348–4360.
13. Guldbrand, L., L. G. Nilsson, and L. Nordenskiöld. 1986. A Monte Carlo simulation study of electrostatic forces between hexagonally packed DNA double helices. *J. Chem. Phys.* 85:6686–6698.
14. Tang, J. X., and P. A. Janmey. 1996. The polyelectrolyte nature of F-actin and the mechanism of actin bundle formation. *J. Biol. Chem.* 271:8556–8563.
15. Bloomfield, V. A. 1997. DNA condensation by multivalent cations. *Biopolymers.* 44:269–282.
16. Levin, Y. 2002. Electrostatic correlations: from plasma to biology. *Rep. Prog. Phys.* 65:1577–1632.
17. Zhang, R., and B. Shklovskii. 2005. The pulling force of a single DNA molecule condensed by spermidine. *Phys. A. Stat. Mech. Appl.* 349:563–570.

18. Levental, I., P. A. Janmey, and A. Cēbers. 2008. Electrostatic contribution to the surface pressure of charged monolayers containing polyphosphoinositides. *Biophys. J.* 95:1199–1205.

19. Travesset, A., and S. Vangaveti. 2009. Electrostatic correlations at the Stern layer: physics or chemistry? *J. Chem. Phys.* 131:185102.

20. Weeks, J. D., D. Chandler, and H. C. Andersen. 1971. Role of repulsive forces in determining the equilibrium structure of simple liquids. *J. Chem. Phys.* 54:5237–5247.

21. Plimpton, S. 1995. Fast parallel algorithms for short-range molecular dynamics. *J. Comput. Phys.* 117:1–19.

22. Hoover, W. G. 1985. Canonical dynamics: equilibrium phase-space distributions. *Phys. Rev. A.* 31:1695–1697.

23. Hockney, R. W., and J. W. Eastwood. 1988. Computer Simulation Using Particles. Taylor and Francis, London, UK.

24. Flanagan, L. A., C. C. Cunningham, …, P. A. Janmey. 1997. The structure of divalent cation-induced aggregates of PIP_2 and their alteration by gelsolin and τ. *Biophys. J.* 73:1440–1447.

25. Shah, D. O., and J. H. Schulman. 1965. Binding of metal ions to monolayers of lecithins, plasmalogen, cardiolipin, and dicetyl phosphate. *J. Lipid Res.* 6:341–349.

26. Marrink, S. J., A. H. de Vries, and A. E. Mark. 2004. Coarse grained model for semiquantitative lipid simulations. *J. Phys. Chem. B.* 108:750–760.

27. Lifshitz, I., and V. Slyozov. 1961. The kinetics of precipitation from supersaturated solid solutions. *J. Phys. Chem. Solids.* 19:35–50.

28. Kielland, J. 1937. Individual activity coefficients of ions in aqueous solutions. *J. Am. Chem. Soc.* 59:1675–1678.

29. Volkov, A. G., S. Paula, and D. W. Deamer. 1997. Two mechanisms of permeation of small neutral molecules and hydrated ions across phospholipid bilayers. *Bioelectrochem. Bioenerg.* 42:153–160.

30. Kiriukhin, M. Y., and K. D. Collins. 2002. Dynamic hydration numbers for biologically important ions. *Biophys. Chem.* 99:155–168.

31. Chen, K., W. G. Ellenbroek, …, A. G. Yodh. 2010. Low-frequency vibrations of soft colloidal glasses. *Phys. Rev. Lett.* 105:025501.

32. Reference deleted in proof.

33. Lee, K.-C., I. Borukhov, …, M. J. Stevens. 2004. Effect of mono- and multivalent salts on angle-dependent attractions between charged rods. *Phys. Rev. Lett.* 93:128101.

34. Christian, D. A., A. Tian, …, D. E. Discher. 2009. Spotted vesicles, striped micelles and Janus assemblies induced by ligand binding. *Nat. Mater.* 8:843–849.